

Splice-variant changes of the $Ca_v3.2$ T-type calcium channel mediate voltage-dependent facilitation and associate with cardiac hypertrophy and development

Laurence S. David, Esperanza Garcia, Stuart M. Cain, Elana M. Thau, John R. Tyson and Terrance P. Snutch*

Michael Smith Laboratories; University of British Columbia; British Columbia, Canada

Key words: voltage-dependent facilitation, alternative splicing, T-type calcium channel, hypertension, cardiac hypertrophy

Abbreviations: Ca, calcium; Ba, barium; cDNA, complementary DNA; E-C, excitation and contraction; HW/BW, heart weight/body weight; HVA, high voltage-activated; $I_{Ca,T}$, T-type calcium channel current; NFAT, nuclear factor of activated T-cells; ORF, open reading frame; PCR, polymerase chain reaction; qRT-PCR, quantitative real time polymerase chain reaction; RT-PCR, reverse transcription polymerase chain reaction; SHR, Spontaneously Hypertensive Rats; VDF, voltage-dependent facilitation; WKY, Wistar-Kyoto Rats

Low voltage-activated T-type calcium (Ca) channels contribute to the normal development of the heart and are also implicated in pathophysiological states such as cardiac hypertrophy. Functionally distinct T-type Ca channel isoforms can be generated by alternative splicing from each of three different T-type genes ($Ca_v3.1$, $Ca_v3.2$, $Ca_v3.3$), although it remains to be described whether specific splice variants are associated with developmental states and pathological conditions. We aimed to identify and functionally characterize $Ca_v3.2$ T-type Ca channel alternatively spliced variants from newborn animals and to compare with adult normotensive and spontaneously hypertensive rats (SHR). DNA sequence analysis of full-length $Ca_v3.2$ cDNA generated from newborn heart tissue identified ten major regions of alternative splicing, the more common variants of which were analyzed by quantitative real-time PCR (qRT-PCR) and also subject to functional examination by whole-cell patch clamp. The main findings are that: (1) cardiac $Ca_v3.2$ T-type Ca channels are subject to considerable alternative splicing, (2) there is preferential expression of $Ca_v3.2(-25)$ splice variant channels in newborn rat heart with a developmental shift in adult heart that results in approximately equal levels of expression of both (+25) and (-25) exon variants, (3) in the adult stage of hypertensive rats there is both an increase in overall $Ca_v3.2$ expression and a shift towards expression of $Ca_v3.2(+25)$ containing channels as the predominant form and (4) alternative splicing confers a variant-specific voltage-dependent facilitation of $Ca_v3.2$ channels. We conclude that $Ca_v3.2$ alternative splicing generates significant T-type Ca channel structural and functional diversity with potential implications relevant to cardiac developmental and pathophysiological states.

Introduction

Alternative splicing is a ubiquitous post-transcriptional mechanism for generating diversity from individual genes and significantly expands the functional repertoire of eukaryotic cells.^{1,2} Greater than half of known human genes are subject to alternative splicing³ and splice-variant expression patterns often correlate with specific developmental stages as well as specific physiological and pathophysiological states.⁴⁻⁷ Cardiovascular diseases have been associated with altered regulation of alternative splicing and changes in the expression ratio of functionally relevant proteins, including some voltage-activated calcium (Ca) channels.⁸⁻¹¹

The expression of distinct Ca channel subtypes contributes to mechanical and electrophysiological functioning of different regions of the heart.^{12,13} However, the identification and temporal and spatial expression patterns of alternatively spliced variants of most Ca channel family members expressed in cardiac tissue has yet to be reported. Low voltage-activated T-type Ca channel currents ($I_{Ca,T}$) play a critical role in spontaneous diastolic depolarization¹⁴ and have also been suggested to regulate the cell cycle and differentiation of cardiac myocytes.¹⁵ Of the three genes encoding T-type channels in mammals, the $Ca_v3.1$ and $Ca_v3.2$ isoforms have been identified as underlying cardiac $I_{Ca,T}$.^{16,17} Both the $Ca_v3.1$ and $Ca_v3.2$ T-types are expressed in atrial and

*Correspondence to: Terrance P. Snutch; E-mail: snutch@msl.ubc.ca

Submitted: 06/16/10; Revised: 06/29/10; Accepted: 06/30/10

Previously published online: www.landesbioscience.com/journals/channels/article/12874

DOI: 10.4161/chan.4.5.12874

ventricular tissues during embryonic and neonatal periods¹⁸⁻²⁰ but by the adult stage $Ca_v3.2$ levels become significantly reduced and $Ca_v3.1$ becomes the predominant cardiac isoform, albeit mainly being restricted to pacemaker cells.^{16,21} In addition to developmental regulation, there is an overall increase in functional $I_{Ca,T}$ under pathological conditions such as post-myocardial infarction and cardiac hypertrophy and both $Ca_v3.1$ and $Ca_v3.2$ T-type Ca channels have been reported to be re-expressed in adult ventricle of diseased hearts.²²⁻²⁶ Specific expression of the $Ca_v3.2$ T-type channel has also been associated with the pathogenesis of pressure overload-induced cardiac hypertrophy in mice.²⁷

All three T-type Ca channel genes are known to be subject to alternative splicing.^{18,28-35} In human fetal and adult brains, $Ca_v3.1$ was shown to have 15 sites subject to alternative splicing,³⁰ while two sites of alternative splicing have been reported to date for the human $Ca_v3.3$ channel.^{29,32} Examining human fetal brain and partial length splice-variant analysis, $Ca_v3.2$ channels were shown to be alternatively spliced at 12 to 14 sites.³⁵ Human uterine and testicular $Ca_v3.2$ T-Ca channels have similarly been found to be alternatively spliced, particularly in the domain III-IV linker region.^{31,34} In a number of these instances, alternative splicing has been shown to affect T-type channel biophysical properties.^{31,34,35} To date, there has been no report concerning cardiac $Ca_v3.2$ T-type channel alternative splicing. A goal of the current study was to describe structural and functional composition of $Ca_v3.2$ channel variation in cardiac tissue from newborn rats and to then compare that with the splice-variant profile from adult heart. Additionally, we hypothesized that under certain pathological conditions there might be changes in $Ca_v3.2$ T-type channels in both overall expression and the level of specific splice variants. Profiling of splice variants was performed using both short amplicon scanning and full-length cDNA screening and combined with quantitative RT-PCR (qRT-PCR) using cardiac samples from newborn and adult male Wistar rats, as well as from hypertrophic spontaneously hypertensive rats (SHR) and age and sex-matched normotensive Wistar Kyoto (WKY) animals. The study demonstrates developmental changes in the expression pattern of the most abundant alternatively spliced $Ca_v3.2$ transcripts in rat atrial and ventricular tissues. Furthermore, altered transcript ratios of the predominant $Ca_v3.2$ isoforms in the left ventricle of adult spontaneously hypertensive rats (SHR) were found to correlate with histopathological signs and the expression of molecular markers of pathological hypertrophy. In addition to a switch in variants with a distinct recovery from inactivation, we find that a major characteristic of $Ca_v3.2$ splicing is the

generation of T-type Ca channels that exhibit voltage-dependent facilitation (VDF).

Results

Alternative splicing generates multiple $Ca_v3.2$ T-type variants with differential expression across development. Utilizing subtype-specific probes and both qRT-PCR and western blot analyses, the expression of the $Ca_v3.1$, $Ca_v3.2$ and $Ca_v3.3$ T-type isoforms as well as the high voltage-activated (HVA) $Ca_v1.2$ L-type and $Ca_v2.2$ N-type Ca channels was determined in neonatal (P0) and adult atria and ventricle (compared to actin B). **Figure 1A and B** shows that the $Ca_v3.1$ and $Ca_v3.2$ T-types and $Ca_v1.2$ L-type Ca channels were robustly expressed at the RNA and protein levels in both cardiac chambers of neonate heart. Contrastingly, in adult animals the expression of both T-type isoforms was significantly lower in the ventricle while the level of expression of the $Ca_v1.2$ L-type remained high in both adult heart chambers. Neither the $Ca_v3.3$ T-type nor $Ca_v2.2$ N-type channels were expressed at appreciable levels in neonate or adult heart chambers (**Fig. 1A**).

The rat $Ca_v3.2$ genomic locus spans ~110,000 kb on chromosome 10 (NCBI, NC 005109; Ensembl, ENSRNOT00000048392). In order to identify $Ca_v3.2$ splice variants expressed in neonate heart, comprehensive transcript screening was initially performed using short amplicon scanning (**Fig. 1C**). The reference $Ca_v3.2$ transcript used in this study corresponds to a transcript containing 35 exons across 7,862 bp and encoding 2,365 amino acids; Ensembl, ENSRNOT00000048392. Distinct from previous reports examining limited portions of the $Ca_v3.2$ channel for variability,^{31,34,35} the entire open reading frame (ORF) of rat cardiac $Ca_v3.2$ transcripts was subject to systematic splice-variant analysis. A total of 11 overlapping PCR amplifications each covering at least two exons and generating products between ~450 and ~1,070 base pairs were subcloned and between 40 and 203 individual cDNAs from each of the amplicon reactions were subject to DNA sequence analysis (**Fig. 1C**). Sequences were searched against available databases and aligned with rat $Ca_v3.2$ genomic (NCBI, NC 005109 and Ensembl, ENSRNOT00000048392) and cDNA (NM_153514) sequences.

Twenty five in-frame/carboxyl variants occur at 10 distinct sites in the $Ca_v3.2$ protein (**Fig. 2 and Suppl. Table 3**). Analysis of 392 short amplicon cDNAs generated from neonate atrial RNA identified six in-frame and truncated carboxyl(C-) terminus variants compared to the parental $Ca_v3.2$ channel: called

Figure 1 (See opposite page). Ca channel expression in rat cardiac tissues and identification of $Ca_v3.2$ alternative splice variants. (A) Shows the relative mRNA expression of the T-type Ca_v3 and the high-voltage activated $Ca_v1.2$ and $Ca_v2.2$ Ca^{2+} channels obtained using qRT-PCR to compare the overall level of isoform expression between newborn and adult cardiac tissues. Adult thalamic tissue is shown for comparison. Cardiac tissue displays high levels of expression of $Ca_v1.2$ and T-type $Ca_v3.1$ and $Ca_v3.2$, whereas neuronal $Ca_v2.2$ is negligible. Both $Ca_v3.1$ and $Ca_v3.2$ Ca^{2+} channels are expressed in cardiac tissues but a significant reduction was observed in adult ventricles, compared to newborn cardiac chambers. Relative amounts were compared to actin B. All experiments were done using 3–6 rats. Error bars show standard error. (B) Western blot analysis showing a significant level of $Ca_v1.2$ isoform protein expression at both developmental stages, whereas $Ca_v3.1$ and $Ca_v3.2$ are prominently expressed only in newborn tissues. In the adult heart T-type channel proteins are moderately expressed in atria and at much lower levels in the ventricle. (C) Is a schematic of the $Ca_v3.2$ protein sequence to illustrate the strategy used to identify alternative splice variants. Numbers along the peptide sequence indicate the exon number (total of 35) and numbers on filled bars correspond to the short amplicon overlapping PCR reaction sequences used for exon scanning (bottom left). Horizontal arrows at N- and C-terminus of the channel correspond to the full-length amplification (bottom right). See Materials and Methods for details.

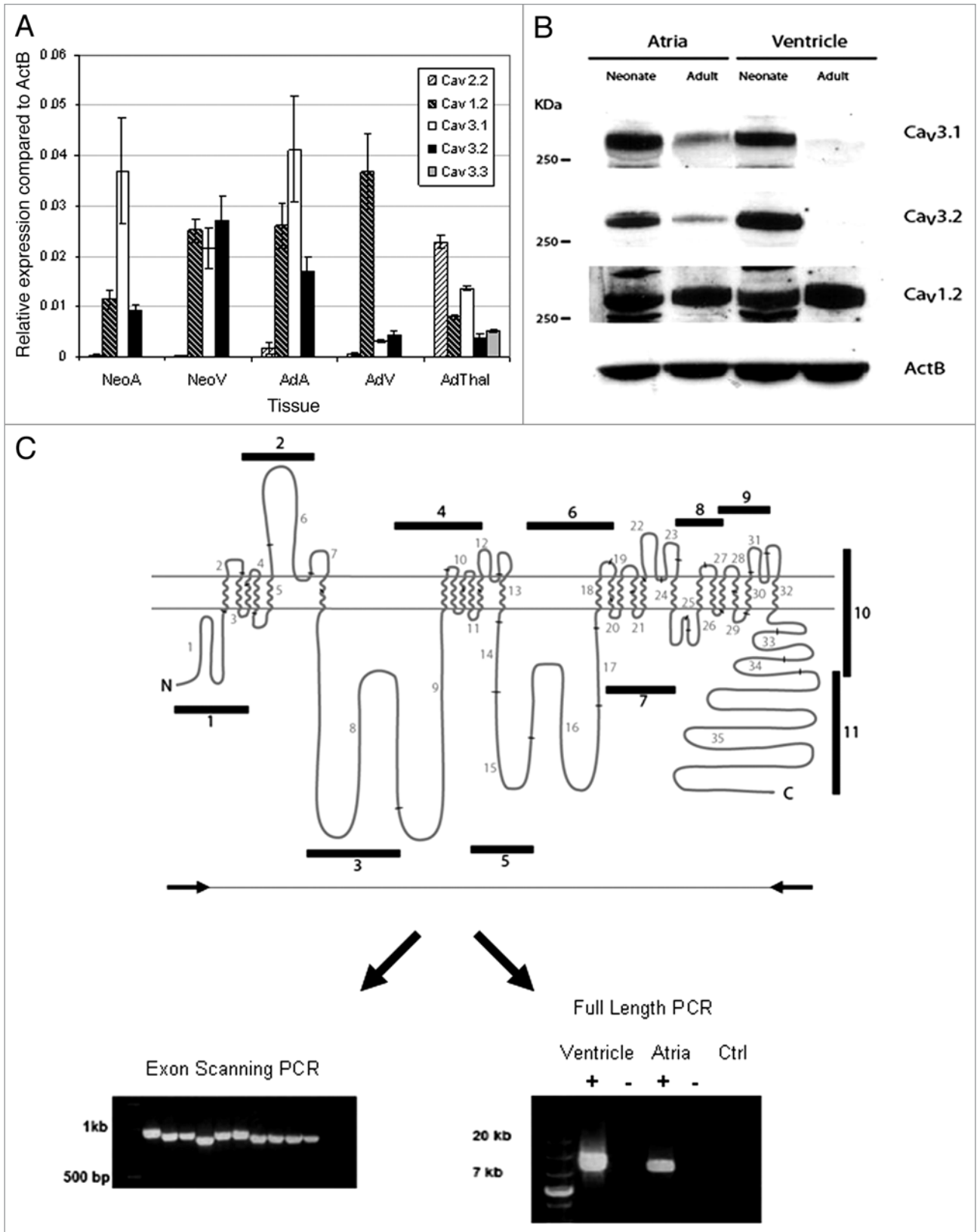


Figure 1. For figure legend, see p. 376..

8a/9a, 20a, -25, 35a, 35c and Δ 210 (Fig. 2). Further analysis of 557 short amplicon cDNAs from neonate ventricle identified 14 in-frame variants and truncated C-terminus compared to the parental $\text{Ca}_v3.2$ channel, ten of which were unique to the neonate ventricular RNA: called variants 1a, -7, 8b, 8c, 28a/29a, 33b/34a, 35b, 35e, Δ 214, Δ 210 and Δ 304, and four of which had also been identified in neonate atria (8a/9a, 20a, -25, Δ 210; Fig. 2). In order to put the individual amplicon variants into context, full-length $\text{Ca}_v3.2$ cDNA was amplified from both atria and ventricle neonate RNA and 56 individually isolated full-length ventricle cDNAs and 50 full-length atria cDNAs were subject to complete DNA sequencing. In addition to placing some of the amplicon variants into their larger expression context, the full-length analyses identified a further eight $\text{Ca}_v3.2$ channel in-frame variants: called 1b, 7a/8d, 9c, 20b, 24a, 33a, 34b and 35d (Fig. 2).

Alternative splicing mechanisms associated with the identified variants are suggested to include deletion and insertion of cassette exons, alternative donor/splice sites, splicing within exons and retained introns.¹ In the amino-terminus, in-frame deletions within exon 1 result in removal of either 16 amino acids (variant 1a) or 8 amino acids (variant 1b). Further downstream, the domain I-II linker region possesses a high degree of variation with five distinct isoforms identified; variants 8b, 8c, 7a/8d, 8a/9a and 9c. An example of a canonical cassette-type exon is the inclusion (+) or exclusion (-) of exon 25 encoding residues in the domain III-IV linker, notable as a site of splice variation previously implicated in regulating voltage-dependent properties of $\text{Ca}_v3.2$ channels.^{31,34-36} In this same region, further neonate cardiac variation results from the partial insertion of 24 nucleotides to the end of exon 24 (called variant 24a).

In domain III, splicing due to an alternate splice acceptor site internal to exon 20 (variant 20a) leads to a 15 amino acid deletion in the cytoplasmic IIIS2-IIIS3 region and the partial insertion of intron 20 (20b) confers a 7 amino acid insertion (SPLPGCR) in domain III S3 (Fig. 2). In domain IV, the use of alternate donor and acceptor splice sites in exons 28 and 29 respectively results in an in-frame deletion of 39 amino acids in domain IV S4 (called 28a/29a). The most extensively spliced region in $\text{Ca}_v3.2$ channels expressed in neonate heart occurs at the carboxyl-terminus and including the parental variant could result in up to 12 distinct carboxyl-terminal isoforms. The newly identified variants include 33a, Δ 214, Δ 210, Δ 304, 33b/34a, 34b, 35a, 35b, 35c, 35d and 35e. The first four of these terminate at the same stop codon (last four amino acids, DEPV) whereas the remaining seven result in alternative carboxyl stop sites, all of which except 33a are shorter versions of the canonical carboxyl-terminus. The 33a splice variant contains the longest carboxyl-terminus due to inclusion of 5 additional amino acids (PPSPQ) at the proximal end.

There are several contextually noteworthy aspects evident from the 106 full-length $\text{Ca}_v3.2$ cDNAs analyzed. Variants 1b, 7a/8d, 9c, 20a, 24a, 33a and Δ 214 always occurred in combination with the (-)25 exon splice variant whereas the 34b isoform occurred in combination with the (+)25 variant. Further, variant 35a was found in combination with either of the (+) or (-) exon

25 splice isoforms. In the full-length $\text{Ca}_v3.2$ cDNA there were a number of combinations of individual exonic variants: e.g., 20b/-25/33a and 20a/-25/35d. Generally, across both the amplicon and full-length analyses the majority of the $\text{Ca}_v3.2$ variants were found to be expressed in either atria or ventricle with a smaller portion being expressed in both chambers (8a/9a, 20a, \pm 25, 35a and Δ 210).

From the combined short amplicon scanning and full-length cDNA analyses, six distinct variant regions were chosen for more in-depth expression analysis in newborn and adult heart chambers by qRT-PCR: $\text{Ca}_v3.2$ (8b) in the domain I-II linker, $\text{Ca}_v3.2$ (20a) between domain IIIS2 and IIIS3, $\text{Ca}_v3.2$ (\pm exon 25) in the domain III-IV linker and three carboxyl-terminal variants— $\text{Ca}_v3.2$ (33a), $\text{Ca}_v3.2$ (Δ 214) and $\text{Ca}_v3.2$ (35a) located at the proximal, middle and distal portions of the carboxyl-terminus (Fig. 3).

In T-type Ca channels the cytoplasmic regions mentioned above have been implicated in gating,^{28,37} surface expression³⁷ and G-protein-dependent regulation.^{38,39} For some variant positions the reference isoform predominates in both neonate and adult and in both chambers (Fig. 3), while in other instances there is clear evidence that both variants are co-expressed at different levels (e.g., \pm 25, 35a vs. ref.). Of the six $\text{Ca}_v3.2$ variants analyzed by qRT-PCR only the (\pm) exon 25 showed a significant difference in relative abundance across newborn and adult hearts and in both atria and ventricle (Fig. 3C).

In the human brain, testis and uterus the $\text{Ca}_v3.2$ exon 26, which is homologous to the exon 25 described here, has been previously implicated in affecting activation, channel availability and recovery from inactivation.^{31,34,35} It was therefore of interest to target this variant region for more in-depth transcript copy number analyses in the heart. Figure 4 shows the transcript copy numbers of $\text{Ca}_v3.2$ (+25) and (-25) exon splice variants normalized to rat ActB. In neonate heart the exclusion of exon 25 occurred at a level 7 to 8 fold higher in atria and ventricle tissues compared to (+25) exon variant transcripts. Contrastingly, in adult atria the relative copies of (+25) exon variant transcripts were increased while adult ventricular (-25) transcripts decreased such that overall the ratio of (+25) to (-25) variants in both adult heart chambers was approximately equal (Fig. 4). Taken together, there appears to be a significant developmental- and chamber-specific mechanism regulating the relative expression of $\text{Ca}_v3.2$ (+25) and (-25) variant channels.

Exclusion of exon 25 confers voltage-dependent facilitation and accelerates recovery from inactivation. The full-length cDNA screening revealed that $\text{Ca}_v3.2$ channel variants in neonate heart predominantly occur in the context of exclusion of exon 25 (Figs. 3 and 4). In this regard, several full-length variants in the context of the (-25) isoform were analyzed following heterologous expression in HEK cells using whole-cell patch-clamp. Biophysical characterization was performed on the following variants identified by full-length cDNA screening: $\text{Ca}_v3.2$ (20a/-25), $\text{Ca}_v3.2$ (-25), $\text{Ca}_v3.2$ (+25), $\text{Ca}_v3.2$ (33a/-25), $\text{Ca}_v3.2$ (Δ 214/-25), $\text{Ca}_v3.2$ (35a/-25) and $\text{Ca}_v3.2$ (35a/+25). We also analyzed the $\text{Ca}_v3.2$ (8b/-25) variant which was identified by short amplicon screening. This variant is located at the I-II

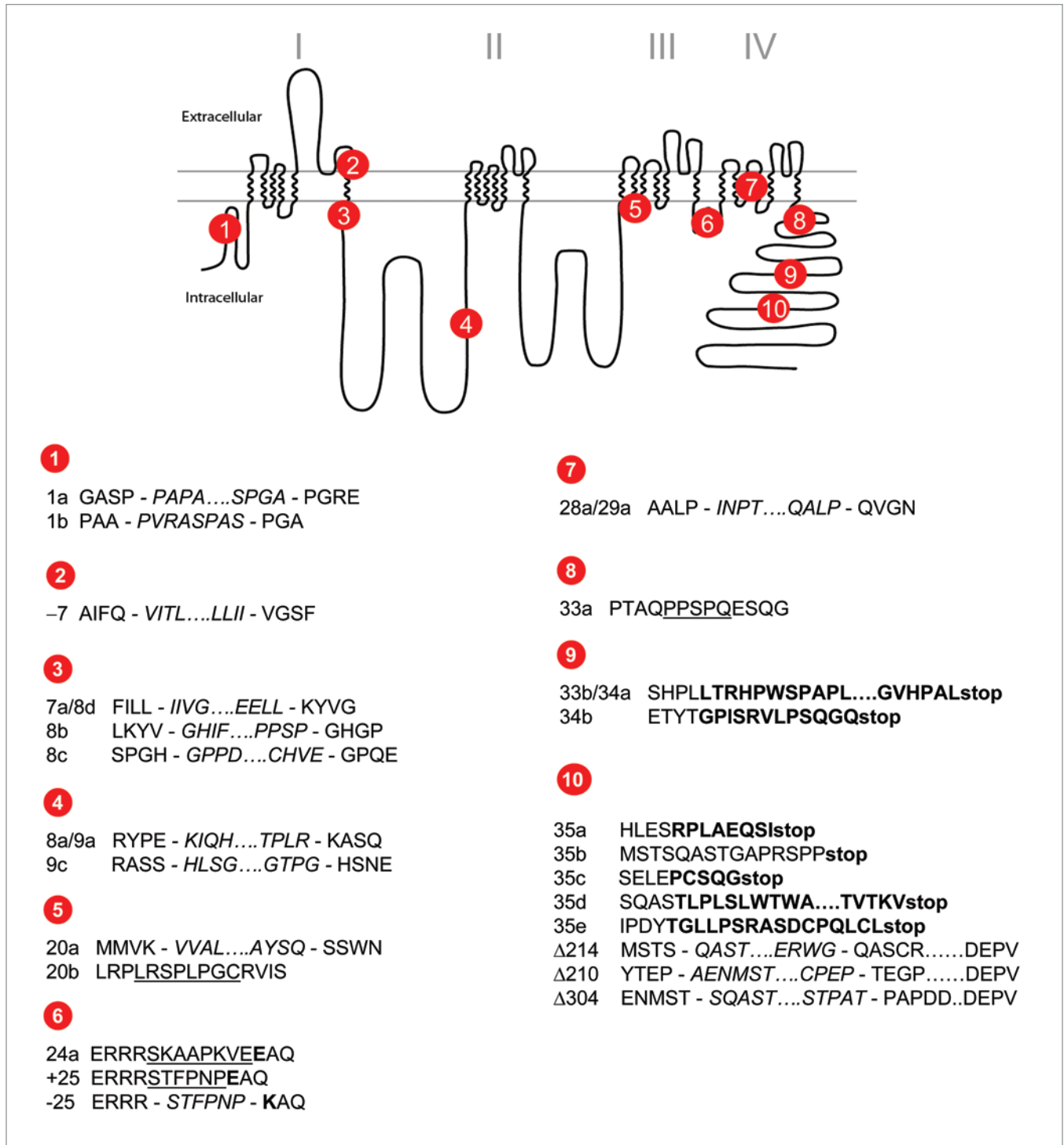


Figure 2. Topology of $Ca_v3.2$ channel showing the location of all in-frame and truncated carboxyl terminal variants. Twenty five identified in-frame and truncated carboxyl-terminus $Ca_v3.2$ variants are located at 10 different sites as indicated in the diagram. The amino acid sequences (single letter code) resulting from each alteration are depicted below. Alternative splice variants are named after the alternatively spliced exons and letters after the exon number correspond to the different variants in that particular exon. (-) and (+) correspond to the absence and the presence of the indicated exon. The symbol Δ followed by a number (n) refer to a deletion n amino acid. When alternative splicing affects consecutive exons, the variants are named using both exon designations separated by a slash. All sequences were aligned using published rat $Ca_v3.2$ genomic and mRNA sequences (NCBI, NC 005109; Ensembl, ENSRN00000048392; and NM_153514). Italicized, underlined and bold indicate deletion, insertion and alternative sequences, respectively. A dash (-) in the peptide sequences correspond to the start and end of deleted amino acids. Out of frame splice variants resulting into premature chain termination, hemichannels or interdomain truncations are not shown.

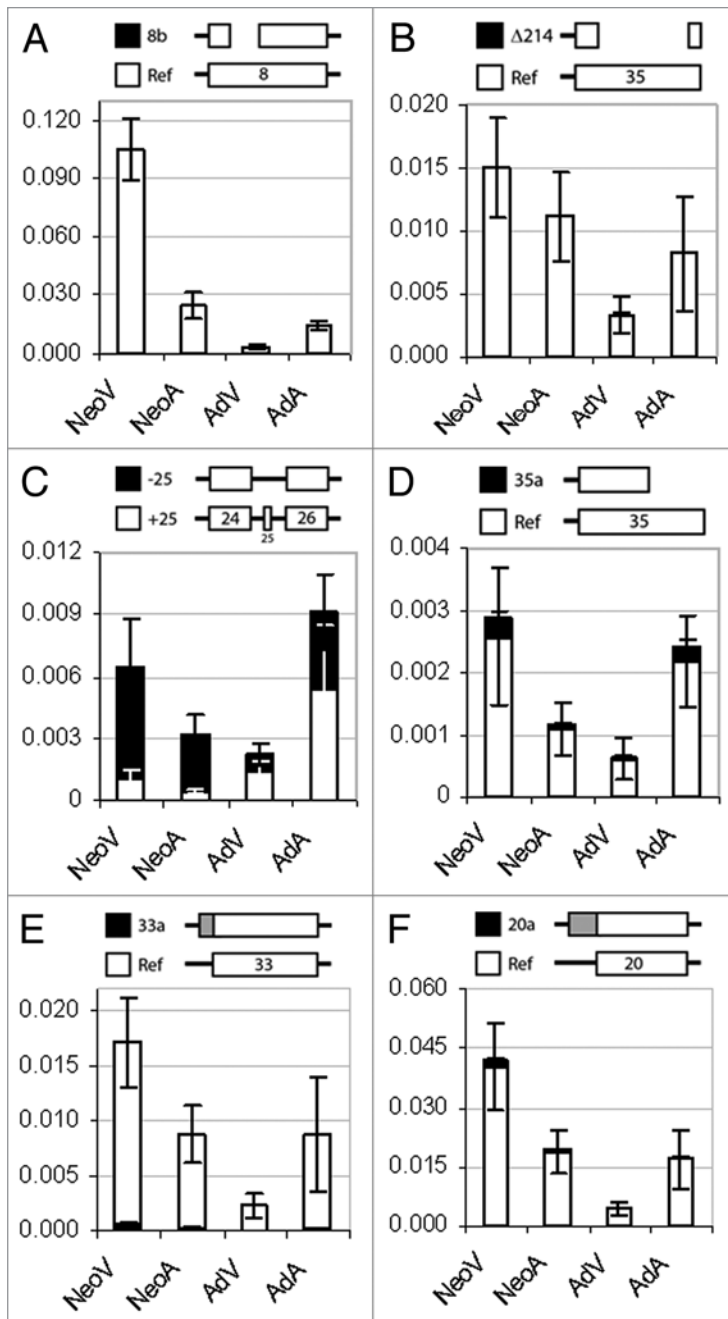


Figure 3. Differential expression of $Ca_v3.2$ T-type Ca channel alternative splice variants in newborn and adult cardiac tissues. Relative mRNA levels of $Ca_v3.2$ splice variants were obtained by qRT-PCR and compared at two developmental stages. Alternative splice variants 8b (A), $\Delta 214$ (B), -25 (C), 35a (D), 33a (E) and 20a (F) display different levels of expression in neonatal and adult atria and ventricle. The (-25) variant is the most abundant in neonate while both (+) and (-) exon 25 variants are present in approximately equal amounts in adult heart. Experiments were performed using 3–6 rats for each sample and qRT-PCR reactions were performed in triplicate. Error bars correspond to standard error. A schematic representation of each splice variant is shown in each graph. Gray box represents an alternative start to a given exon, gaps represent deletions and open boxes the reference sequence of each exon. Y-axis scale represents relative expression compared to ActB. NeoA (neonatal atria), NeoV (neonatal ventricle), AdA (adult atria), AdV (adult ventricle). Each variant probe was checked for specificity against its parental cDNA before qRT-PCR analysis.

linker, a region implicated in controlling gating and plasma membrane surface expression.³⁷

Examination of current densities from macroscopic Ca currents showed that $Ca_v3.2(+25)$, $Ca_v3.2(\Delta 214/-25)$, $Ca_v3.2(35a/-25)$ and $Ca_v3.2(8b/-25)$ variants had significantly higher current densities (30.34 ± 4.13 , 31.60 ± 5.95 , 38.39 ± 5.70 , 66.14 ± 17.45 pA/pF, respectively) compared with the $Ca_v3.2(-25)$ variant (21.64 ± 1.88 pA/pF). The parameters of voltage-dependent gating properties are summarized in Table 1. Overall, exon 25 containing variant channels displayed small but significant differences in the voltage dependence of activation. $Ca_v3.2(8b/-25)$ and $Ca_v3.2(+25)$ showed ~ 10 mV and ~ 5 mV leftward shifts in the V_{50act} relative to $Ca_v3.2(-25)$. In regards to steady-state inactivation, a 10 mV hyperpolarizing shift was observed when $Ca_v3.2(8b/-25)$ ($V_{50inact} = -75.7 \pm 0.3$ mV) was compared with $Ca_v3.2(-25)$ ($V_{50inact} = -65.5 \pm 0.3$ mV) (Suppl. Fig. 1). The voltage dependence of deactivation as well as the kinetics of Ca currents generated by expressing the splice variants was also analyzed. Only the proximal carboxyl-terminus splice variant $Ca_v3.2(33a/-25)$ showed changes in the kinetics of activation and inactivation compared to $Ca_v3.2(-25)$ (Table 1). All seven variants examined showed similar voltage-dependence of deactivation (Table 2).

The recovery from inactivation was investigated using a double pulse protocol (Fig. 5A inset) and time constants obtained by fitting a double exponential function are shown in Table 2. $Ca_v3.2(-25)$ channels recovered significantly faster (~ 1 second) from inactivation than $Ca_v3.2(+25)$ channels (~ 2.5 seconds; Fig. 5A and Table 2). Interestingly, compared to $Ca_v3.2(+25)$ channels, $Ca_v3.2(-25)$ channels recover from inactivation to a level greater than 100%, suggesting facilitation (or potentiation) of this variant. The distal carboxyl-terminus variant $Ca_v3.2(35a)$ also displayed significant potentiation when expressed in combination with $Ca_v3.2(-25)$ but not when expressed in a $Ca_v3.2(+25)$ background (Fig. 5A), suggesting that exclusion of exon 25 residues located in the domain III-IV linker are a structural determinant for the observed facilitation. Representative current traces of recovery from inactivation for $Ca_v3.2(-25)$ and $Ca_v3.2(+25)$ variants are shown in Figure 5B and C respectively. In order to further investigate if the potentiation observed in $Ca_v3.2(-25)$ variant could be attributed to VDF, two pulse protocols were used as shown in Figure 5D and F. Percentage of VDF (Fig. 5E) was measured as the ratio of current magnitude evoked by a test pulse at -30 mV applied after a strong depolarizing prepulse ($+120$ mV) over the current magnitude in the absence of prepulse. The time course was determined by increasing the time intervals (from 300 ms to 1,500 ms) between the prepulse and the test pulse (Fig. 5D). Voltage dependence of facilitation was then explored by applying prepulses from -120 mV to $+150$ mV with a constant interpulse interval of 1,200 ms (Fig. 5F). The robust VDF displayed by $Ca_v3.2(-25)$ (50–60%) was absent in the $Ca_v3.2(+25)$ splice variant (Fig. 5E). Furthermore, $Ca_v3.2(35a/-25)$ showed

facilitation properties (50–60%) (data not shown), consistent with an increase in fractional recovery (Fig. 5A) when expressed in the Ca_v3.2(-25) background, but not when expressed in combination with Ca_v3.2(+25), suggesting that exclusion of exon 25 in the rat Ca_v3.2 III-IV linker region is associated with VDF. This property was also observed when barium (Ba) was substituted for Ca in the external recording solution. The degree of relative facilitation for both the Ca_v3.2 (-) and (+) exon 25 splice variants showed no significant difference regardless of whether Ca or barium (Ba) was as the charge carrier thereby affirming the facilitation as being voltage-dependent (Fig. 6). The magnitude of facilitation elicited by strong depolarizing prepulses was also examined in stable cell lines expressing human Ca_v3.1 and Ca_v3.3 isoforms and compared with that observed for the Ca_v3.2(±25) splice variant (Suppl. Fig. 2). Consistent with previous studies,^{40,41} Ca_v3.3 channels display an approximate 20% VDF, significantly smaller than that reported here for Ca_v3.2(-25) variant channels. We did not detect any VDF facilitation for the Ca_v3.1 T-type channel variant examined.

Differential expression of Ca_v3.2(-25/+25) variants in hypertension-associated cardiac hypertrophy. Both the altered expression of T-type Ca channels and electrical properties of cardiomyocytes have been reported to be associated with a number of cardiac disease states.²²⁻²⁶ In order to examine the expression profile of identified cardiac Ca_v3.2 splice variants in diseased heart, cardiac tissue from adult spontaneously hypertensive rats (SHR) was analyzed as described above. Figure 7C and D show a comparison of the quantitative mRNA analysis of Ca_v3.2(±25) splice isoforms in cardiac tissue from normotensive Wistar-Kyoto (WKY) and SHR rats. The hypertrophic phenotype of the SHR animals was confirmed using the two molecular markers SIAT7⁴² and Frzb,⁴³ known to be upregulated in pathological cardiac hypertrophy (Fig. 7B). The pathological phenotype of SHR was further confirmed by the elevation in heart weight/body weight (HW/BW) ratio in SHR animals, compared to age- and sex-matched normotensive Wistar-Kyoto (WKY) rats (data not shown). Also, the occurrence of perivascular and focal interstitial fibrosis, determined using Masson's trichrome technique, was used as an indicator of pathological hypertrophy in ventricular tissue from SHR hearts (Fig. 7A). The quantitative mRNA analysis of rat rSIAT7 and rFrzb showed a ~4–5 fold increase of mRNA levels in hypertrophic SHR compared to normotensive WKY left ventricle (Fig. 7B). Importantly, a significant increase in the relative amount of Ca_v3.2(+25) splice isoform compared to Ca_v3.2(-25) (Fig. 7C and D) results in a shift in the predominant exon 25 splice isoform expressed in hypertrophic SHR, suggesting a splice-specific upregulation of Ca_v3.2 mRNA transcripts during pathological hypertrophic heart remodeling, in addition to an overall increase in total Ca_v3.2 isoform expression.

Discussion

The present study provides evidence for the differential regional and temporal expression of alternatively spliced Ca_v3.2 T-type Ca channels in rat heart. Alternative splice variants span the entire Ca_v3.2 channel with the carboxyl-terminal region being

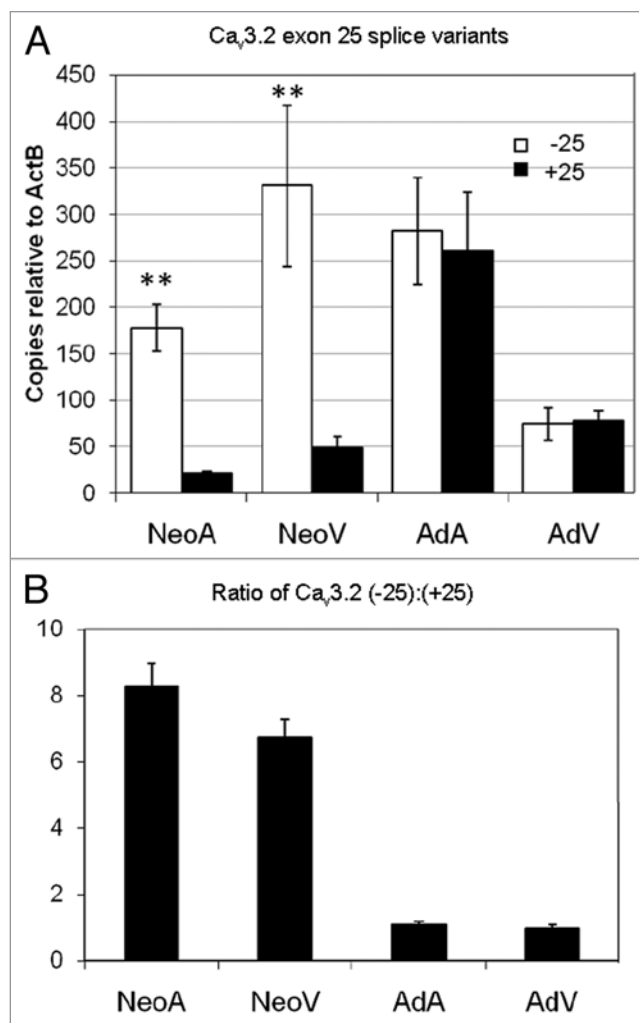


Figure 4. Spatial and developmental changes in the expression of the Ca_v3.2 (+25) and (-25) exon splice variants. (A) shows developmental differences in the relative number of transcript copies of Ca_v3.2 (+25) and (-25) splice variants. There is preferential expression of (-25) Ca_v3.2 variant channels compared to (+25) alternative splice variant in newborn ventricle and atria. Approximately the same level of mRNA expression of both exon 25 variants was observed in adult heart. The developmental shift in the proportion of exon 25 variants expressed in cardiac chambers is shown on (B). (B) A ~7- to 8-fold difference in the ratio of (-25) over (+25) exon variant copy number was obtained using specific qRT-PCR probes and titration against quantified cDNA clones from each respective variant and then normalized relative to rActB levels. Error bars show standard error. t-tests were performed to measure significant differences. **p < 0.01. NeoA (neonatal atria), NeoV (neonatal ventricle), AdA (adult atria), AdV (adult ventricle).

the most extensively spliced domain. Examining cardiac regional and developmental expression patterns by qRT-PCR, the inclusion or exclusion of exon 25 in the domain III-IV linker generates the most distinct splice variant expression profile in cardiac Ca_v3.2 channels. Further, examining hypertrophic heart from adult SHR animals, a significant overall upregulation of Ca_v3.2 expression was observed and occurred in the context of a change in the ratio of the exon (±) 25 splice variants. Heterologous expression analysis of predominant splice variants demonstrated

Table 1. Gating properties of Ca_v3.2 alternative splice variants

	Activation				Inactivation				
	V _{50act} (mV)	k (mV)	τ _{act} (ms)	n	V _{50inact} (mV)	k (mV)	n	τ _{inact} (ms)	n
Ca _v 3.2(-25)	-41.4 ± 0.5	-7.0 ± 0.3	21.8 ± 0.9	34	-65.5 ± 0.3	4.5 ± 0.2	14	5.6 ± 0.5	30
Ca _v 3.2(8b/-25)	-51.7 ± 0.4*	-6.5 ± 0.3	18.3 ± 0.9	9	-75.7 ± 0.3*	3.8 ± 0.2	9	4.5 ± 0.5	8
Ca _v 3.2(33a/-25)	-39.2 ± 0.6	-7.7 ± 0.3	39.6 ± 5.5*	11	-63.9 ± 0.2	4.6 ± 0.2	7	3.8 ± 0.3*	8
Ca _v 3.2(Δ214/-25)	-41.2 ± 0.6	-7.7 ± 0.3	25.5 ± 2.5	12	-63.8 ± 0.3	4.8 ± 0.2	6	8.0 ± 1.1	10
Ca _v 3.2(35a/-25)	-44.4 ± 0.5	-6.2 ± 0.3	21.0 ± 2.5	14	-66.5 ± 0.2	4.2 ± 0.2	11	5.6 ± 0.8	15
Ca _v 3.2(35a/+25)	-46.6 ± 0.4*	-6.0 ± 0.3	19.5 ± 0.6	10	-68.3 ± 0.1	4.9 ± 0.1	10	5.5 ± 0.7	10
Ca _v 3.2(+25)	-45.7 ± 0.7*	-6.6 ± 0.3	19.5 ± 2.2	23	-67.9 ± 0.2	4.1 ± 0.2	13	5.5 ± 0.5	20

*All variants were compared against Ca_v3.2(-25) and significant differences were calculated using ANOVA p < 0.05.

Table 2. Deactivation and recovery from inactivation of Ca_v3.2 alternative splice variants

	Deactivation		Recovery from Inactivation		
	τ _{deact} (ms)	n	τ ₁ (ms)	τ ₂ (ms)	n
Ca _v 3.2(-25)	17.7 ± 1.0	14	36.6 ± 12.3	325.0 ± 33.4	20
Ca _v 3.2(8b/-25)	22.2 ± 1.5	8	50.2 ± 24.2	306.1 ± 36.9	7
Ca _v 3.2(33a/-25)	19.3 ± 1.4	7	47.3 ± 14.9	356.1 ± 33.5	7
Ca _v 3.2(Δ214/-25)	16.6 ± 0.9	5	36.9 ± 12.8	330.9 ± 30.6	6
Ca _v 3.2(35a/-25)	20.4 ± 1.1	8	32.5 ± 12.0	295.3 ± 27.9	15
Ca _v 3.2(35a/+25)	24.2 ± 1.7	10	31.8 ± 2.9	693.8 ± 9.9*	7
Ca _v 3.2(+25)	20.0 ± 0.8	12	32.3 ± 7.6	629.9 ± 25.0*	14

*All variants were compared against Ca_v3.2(-25) and significant differences were calculated using ANOVA p < 0.05.

distinct recovery from inactivation and VDF properties are associated with the exon (±)25 containing variant channels. To our knowledge, this is the first comprehensive study across the full length Ca_v3.2 channel and which also demonstrates splice variation is correlated with cardiac development and the hypertrophic state.

Splice variant specific expression of cardiac Ca_v3.2 Ca channels in development and hypertrophy. Alternative splicing of partial regions of Ca_v3.2 T-type channels has thus far been reported from human fetal brain, testicular and pregnant uterine tissue.^{31,34,35} Here, we examined the entire ORF of rat heart Ca_v3.2 channels using both short amplicon and full-length

cDNA analyses and further examined predominant variants by qRT-PCR and exogenous expression. The results indicate that cardiac Ca_v3.2 channels are subject to extensive alternative splicing, particularly in predicted cytoplasmic regions where second messenger-dependent modulatory and protein-protein interaction sites are primarily located (reviewed in refs. 38 and 39). The cytoplasmic regions of T-type Ca channels are known to affect channel gating,^{28,37} trafficking to the membrane,³⁷ G-protein dependent modulation,^{38,39,44} and regulation by a number of kinases⁴⁵⁻⁴⁷ suggesting that alternative splicing in these regions has the potential for affecting the modulation and functional diversity of cardiac Ca_v3.2 T-type channels.

Figure 5 (See opposite page). Alternative splicing affects the time course of recovery from inactivation and voltage-dependent facilitation of Ca_v3.2 T-type macroscopic currents. (A) The splice variant generated by exclusion of exon 25 (Ca_v3.2(-25), filled squares) displays a faster recovery from inactivation than the Ca_v3.2(+25) variant (upright triangles) enabling Ca_v3.2 channels to recover to more than 100% after a prolonged depolarization. The contribution of carboxyl-tail domain on the recovery from inactivation was explored by expressing both the (+) and (-) 25 exon variants in combination with the (35a) variant. Maximal fraction and time course of recovery from inactivation of 35a/+25 (filled circles) and 35a/-25 (open circles) were determined by the exon 25 variant used as background. A significant increase in fractional recovery was observed when the variant 33a (a five amino acid insertion in the proximal C-terminus) was expressed in combination with the (-25) variant (Ca_v3.2(33a/-25), inverted triangles). Recovery from inactivation was studied with a double-pulse protocol (inset A) using a 400 ms prepulse to -30 mV from a holding potential of -110 mV. After the inactivating prepulse, a 50 ms test pulse to -30 mV was given after varying time period (interpulse interval) between 5 and 5,000 ms. The peak current from the test pulse was plotted as a ratio of maximum pre-pulse current versus interval between pulses. Average data were fitted with a double exponential function to obtain the time constants for the fast (τ₁) and slow (τ₂) components of recovery from inactivation. Representative traces are shown for Ca_v3.2(+25) (B) and Ca_v3.2(-25) (C). The time course of VDF was explored with the protocol showed in (D). A strong depolarization to +120 mV was applied from a holding potential of -100 mV and followed by a 200 ms test pulse to -30 mV with interpulse intervals of 300, 600, 900, 1,200, 1,500 ms. Representative traces illustrate VDF of Ca_v3.2(-25) variant. (E) The current ratio was determined by dividing the current amplitude of the test pulses preceded by a prepulse by that of the test pulse without a prepulse. Robust voltage-dependent facilitation (VDF) was observed in the Ca_v3.2(-25) splice variant (filled squares) compared with Ca_v3.2(+25). VDF was observed with prepulses from 0 mV to +150 mV. Representative traces for Ca_v3.2(-25) VDF and the protocol used are shown on (F). VDF was studied by applying a 200 ms test pulse to -30 mV following a series of depolarizing prepulses from -120 to +150 mV after a time interval of 1.2 sec.

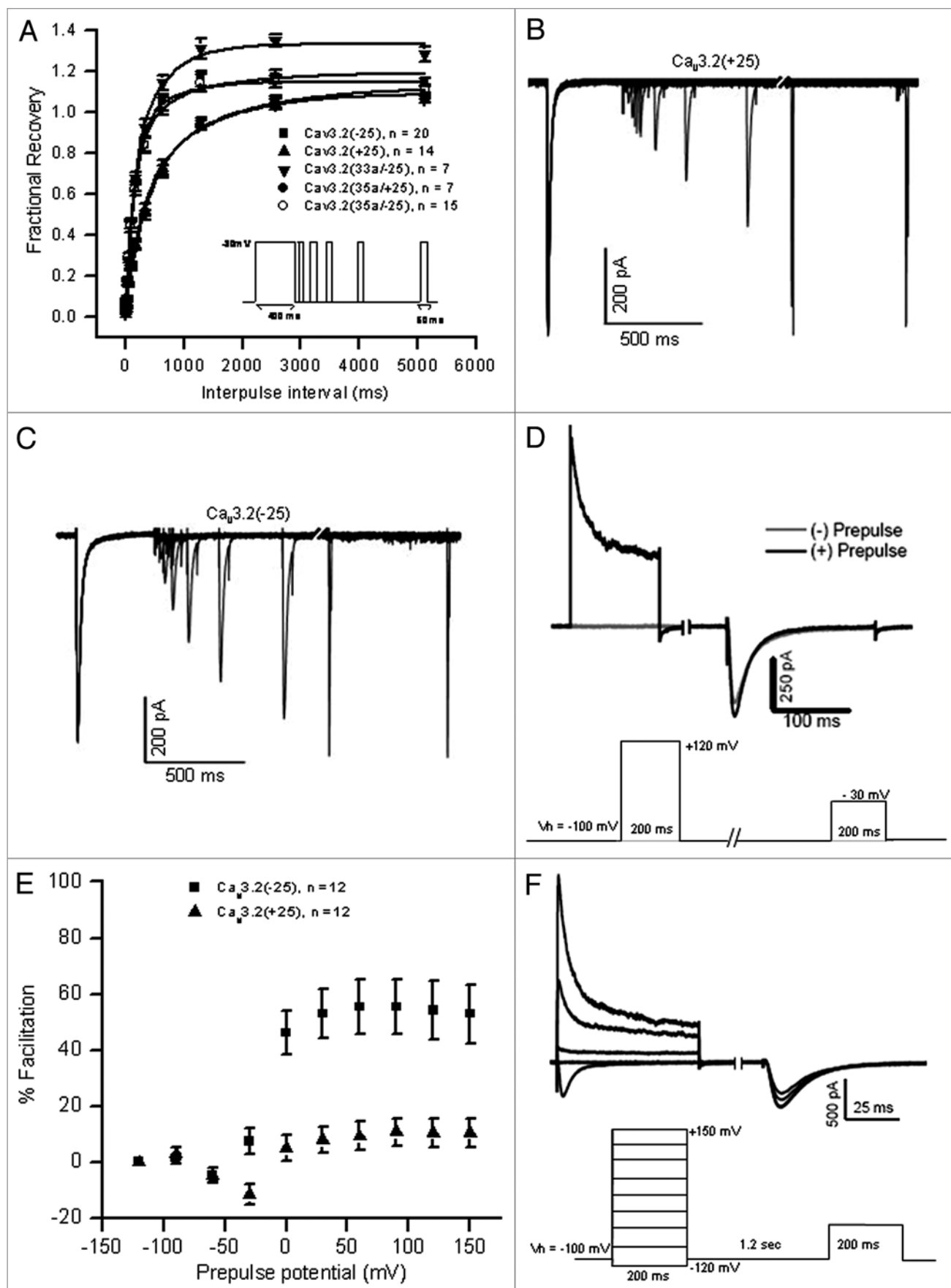


Figure 5. (For figure legend, see p. 382).

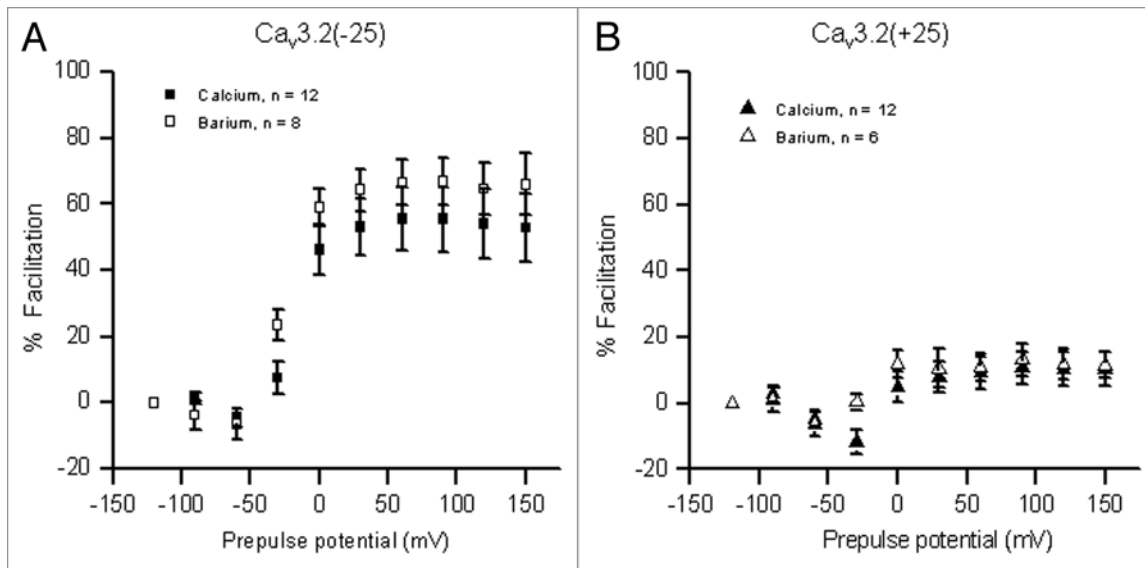


Figure 6. The voltage-dependent facilitation associated $Ca_v3.2(-25)$ T-type Ca channels does not depend upon Ca. The ionic sensitivity of voltage-dependent facilitation was explored using calcium or barium as charge carriers in both the exon 25 (+) and (-) splice variants. The magnitude of relative facilitation observed in $Ca_v3.2(-25)$ (A) and $Ca_v3.2(+25)$ (B) showed no significant difference when currents were recorded in calcium (filled symbols) or barium (open symbols). Data were obtained using the pulse protocol shown in the inserts of Figure 5D and F.

The inclusion or exclusion of the cassette exon 25 encoding residues in the domain III—IV linker was the most common splicing event in cardiac samples. The exclusion of exon 25 is the predominant splice variant in newborn rat heart, being 7- to 8-fold higher than $Ca_v3.2(+25)$ variant channels in newborn cardiac tissue (Fig. 4B). Contrastingly, in adult rat heart the expression of the two variants was approximately equal. A significant reduction in the expression of ventricular $Ca_v3.2(-25)$ splice-variant channels reported here might explain the overall downregulation reported in previous studies for the $Ca_v3.2$ isoform in the adult.^{21,26} However, in the atria, a significant amount of both $Ca_v3.2(+)$ and $(-)$ exon 25 variants was detected (Fig. 4A).

In order to determine whether $Ca_v3.2$ alternative splicing is altered during cardiac remodeling associated with diseased heart, the hypertrophic SHR model was examined. Previous studies have shown that $Ca_v3.2$ T-type channels are generally re-expressed in hypertrophied heart.²³⁻²⁵ The current study addresses for the first time whether there are specific changes in the profile of $Ca_v3.2$ splice-variants in cardiac tissue from hypertension-associated hypertrophic heart. Quantitative analysis showed a preferential expression of the inclusion of (+)25 exon containing variants in the adult hypertrophic heart (Fig. 7C and D). Moreover, the combined increase in expression levels of both exon 25 variants in hypertrophic ventricle could account for the disease-associated re-expression of T-type channels previously reported.²²⁻²⁶

$Ca_v3.2(-25)$ channels display faster recovery from inactivation and voltage-dependent facilitation. Alternative splicing is known to confer distinct electrophysiological properties to T-type Ca channels.^{28,30,31,34,35} Our data examining the cardiac $Ca_v3.2$ channel show significant variant-specific changes in recovery

from inactivation and VDF in association with splicing of exon 25. When compared to $Ca_v3.2(+25)$ variant channels, we find both potentiation and a robust VDF in the rat cardiac $Ca_v3.2$ when exon 25 is absent. The splice-variant specific VDF was also observed when macroscopic currents were recorded using Ba as charge carrier, ruling out a direct calcium-dependent facilitation process (Fig. 6). Of note, native $I_{Ca,T}$ from bullfrog atrial cells and guinea-pig coronary arterial myocytes have both been reported to display VDF properties.⁴⁸⁻⁵⁰ Conversely, Zhong and coworkers reported faster recovery kinetics associated with the homologous exon 26 region in the human fetal brain $Ca_v3.2$ channel although neither facilitation nor potentiation (>100% fractional recovery) were observed.³⁵ VDF has been previously attributed to the cloned human $Ca_v3.3$ ^{40,41} albeit to a much lower degree (~20%) compared to that for the $Ca_v3.2(-25)$ variant channel described here (Fig. 5 and Suppl. Fig. 2).^{40,41}

It is well known that the mammalian heart undergoes significant functional and morphological changes during embryonic and postnatal development. The heart rate, configuration of action potential and excitation-contraction (E-C) coupling all differ considerably between postnatal and adult myocardial tissues.⁵¹⁻⁵⁴ In this regard, age-related differences in the relative expression of $Ca_v3.2$ splice variants displaying significantly different kinetic and gating properties could contribute to the developmental regulation of cardiac Ca homeostasis. As a consequence, splice-specific T-type channel mediated Ca entry could participate in the regulation of important processes in the developing heart such as cardiomyocyte growth, proliferation, hormone secretion and spontaneous activity.^{15,55} In neonate cardiomyocytes, the strong VDF and faster recovery from inactivation of $Ca_v3.2(-25)$ channels may result in increased Ca influx leading to increased electrical activity. Furthermore,

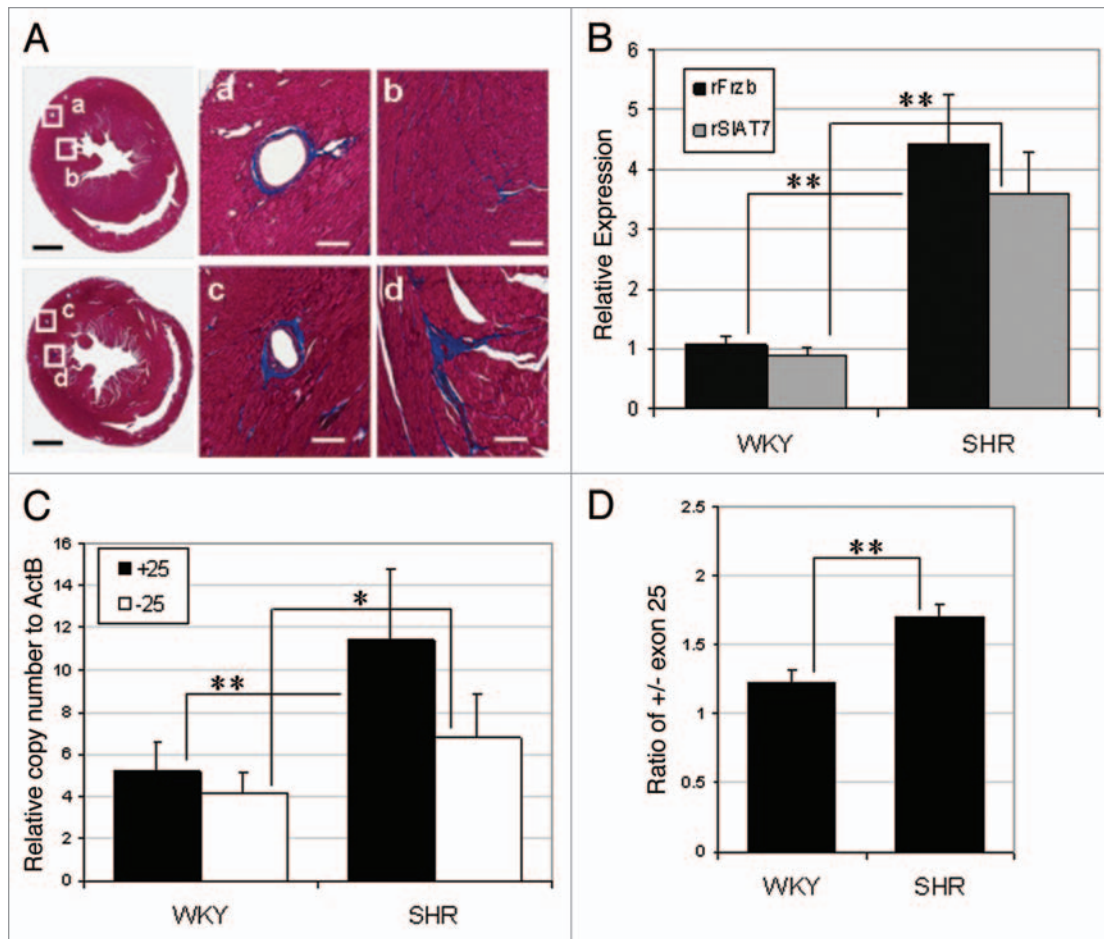


Figure 7. Alteration of $Ca_v3.2$ (+25) and (-25) splice variant expression is associated with the hypertrophic SHR pathological phenotype. (A) Histopathological markers in cardiac tissue from hypertrophic SHRs. Photomicrographs of ventricular sections of cardiac tissue stained with Masson's trichrome show perivascular (c) and interstitial (d) accumulation of fibrillar collagen in SHR heart (lower parts, c and d) compared to the age- and sex-matched normotensive WKY (upper parts, a and b). Leftmost part calibration bar is 2 mm and a–d middle and right parts is 200 μ m. Cardiac tissue was embedded in paraffin, sectioned at 5 μ m and stained by the Masson's trichrome technique. (B) Real time PCR revealed the expression of the rat Frzb (rFrzb) and rat SIAT7 (rSIAT7) hypertrophic markers relative to rActB in cDNA samples generated from left ventricle tissue from adult hypertrophic SHR or adult normotensive WKY. Five individual animals were sampled for each group. The same cDNA samples were used to measure expression of the $Ca_v3.2$ (+25) and (-25) exon splice variants in the SHR and WKY groups. (C) Transcript copies of (+25) and (-25) were calculated from each sample and normalized to rActB. Both variants were upregulated in hypertrophic SHR although the (+25) variant showed more pronounced upregulation indicating the preferential re-expression of (+25) splice variant in cardiac hypertrophy (D). Error bars indicate standard error. t-tests were performed to measure significant differences. ** $p < 0.01$, * $p < 0.05$.

predominant expression of $Ca_v3.2$ (-25) (Fig. 4) might be relevant for E-C coupling in immature myocardium which relies mainly on trans-sarcolemmal transport of Ca for the activation of contractile machinery.⁵⁶ Although the physiological impact of $Ca_v3.2$ splice variation in different regions of the mammalian heart remains to be explored, our study demonstrates that alternative splicing can regulate the effect of strong depolarization on T-type Ca channel gating properties as well as the time course of recovery from inactivation.

Potential relevance to cardiac pathophysiology. Splice variation associated with the cardiac HVA L-type channel encoded by $Ca_v1.2$ has been extensively studied. Of note pharmacologically, splice variation in the $Ca_v1.2$ IS6 segment accounts for the differential dihydropyridine sensitivity of L-type Ca currents in smooth and cardiac tissues.⁵⁷ Further, distinct $Ca_v1.2$ splice

variants expressed in cardiac and smooth muscle contributes to the distinct biophysical properties of native L-type currents in these tissues.^{58–61} Similar to our results presented here for the $Ca_v3.2$ T-type channel, alternative splicing of the $Ca_v1.2$ L-type channel is also suggested to be involved in molecular remodeling associated with cardiovascular disease.^{10,62}

It is tempting to speculate that the preferential upregulation of $Ca_v3.2$ (+25) channels in the heart of hypertrophic SHRs could potentially contribute to electrical remodeling in the hypertrophic ventricle. A higher level of expression of this particular splice variant with its hyperpolarized activation range and higher current density, could predispose the heart to a pro-arrhythmogenic condition, contractile dysfunction and eventually heart failure. Interestingly, a recent study has found evidence implicating $Ca_v3.2$ T-type Ca channel involvement in the pathogenesis of

cardiac hypertrophy via the activation of calcineurin/nuclear factor of activated T cells (NFAT) pathway.²⁷ The preferential upregulation of Ca_v3.2(+25) splice variant channels that we find correlated with cardiac hypertrophy in SHR supports the notion that an enhanced Ca flux associated with expression of this T-type variant might contribute to the hypertrophic signaling pathway.

In summary, we find that alternative splicing of Ca_v3.2 Ca channel results in spatially and temporally expressed T-type cardiovascular variants and that in at least one instance are also associated with the hypertrophic state. The functional variability and compartmentalization of specific Ca_v3.2 splice variants potentially make significant contributions towards cardiac physiology and pathophysiology. In a broader context, it is apparent that examination of single splice variants should not be used to universally infer functional outcomes when looking across physiological and pathological conditions.

Materials and Methods

Animals and tissue preparation. All animal procedures were performed in accordance with Canadian Council on Animal Care guidelines for animal research. Newborn (P0), adult male Wistar (Animal Care Center, University of British Columbia, Canada) and four month old male spontaneously hypertensive rats (SHR) and Wistar Kyoto rats (WKY) (Charles River, Montreal, QC Canada) hearts were utilized in this study. Newborn and adult rats were anaesthetized using halothane (in closed chamber) and inactin (80 mg/kg i.p.), respectively. Rat heart chambers were dissected and washed in Krebs-Ringer solution containing (in mM) 120 NaCl, 4.8 KCl, 1.2 CaCl₂, 1.3 MgSO₄, 25.2 NaHCO₃, 5.8 glucose, 1.2 KH₂PO₄, 20 HEPES, pH 7.4. Krebs-Ringer solution was prepared in diethylpyrocarbonate (DEPC)-treated deionized water and filtered prior to use. The ratio of the heart weight (HW)/body weight (BW) from SHR and WKY was calculated by dividing the total body weight from the heart wet weight. All chemicals used in the study were purchased from Sigma-Aldrich Canada unless otherwise stated.

Histological staining. Four month old male SHR and WKY rats were anaesthetized using 80 mg/kg body weight inactin (Sigma, St. Louis, MO) administered intraperitoneally. Hearts were excised and washed through the aorta with Krebs-Ringer buffer then perfused with 10% cold buffered formalin. Hearts were fixed in formalin for at least 24 hours at 4°C. Samples were processed by Wax-It Histology Services (University of British Columbia, Vancouver, BC Canada). Briefly, cardiac tissues were embedded in paraffin, sectioned at 5 μm and stained using Masson's trichrome technique to detect interstitial fibrosis. The technique uses acid fuchsin-xylydine ponceau for cytoplasmic staining (red), Weigert's hematoxylin for nuclear staining (black) and aniline blue for collagen. High resolution images were obtained by digital scanning of whole slides using Aperio's ScanScope system (Vista, CA).

RT-PCR and short amplicon scanning. Total RNA was prepared individually from five newborn, five SHR and five WKY rats. Each heart sample was homogenized in a sterile glass-Teflon

homogenizer and 1 ml Trizol (Invitrogen). Homogenized samples were incubated at room temperature for 5 minutes followed by adding 200 μL chloroform and incubated at room temperature for another 3 minutes. Samples were spun in table top centrifuge at 11,000 x g for 15 minutes at 4°C. The aqueous phase of the centrifugate was immediately transferred to a clean RNase-free eppendorf tube and 500 μL of isopropanol was added. The centrifugate/isopropanol mixture was incubated at room temperature for 10 minutes to precipitate the RNA. After the incubation, samples were spun at 11,000 x g for 10 minutes at 4°C. The precipitate was washed with 75% ethanol and spun at 7,500 x g for 5 minutes. The supernatant was removed and the final pellets were dried briefly prior to suspension in DEPC-treated deionized water.

For cDNA synthesis, one microgram total RNA was initially treated with DNase to avoid genomic DNA contamination during reverse transcription (RT). Superscript II reverse transcriptase (Invitrogen) was used for the RT. A total of 20 ul reaction volume was prepared containing DNase-treated total RNA, first strand buffer (1X), DTT (10 μM), oligodT (0.5 μg/L), dNTP mix (500 μM), RNaseOUT (40 units) and RT (200 units).

Primer pairs were used to amplify small polymerase chain reaction amplicons covering overlapping regions of the entire Ca_v3.2 open reading frame. The oligonucleotides used in exon scanning are summarized in **Supplemental Table 1**. There were 11 overlapping PCR amplifications with each reaction covering at least two exons and generating products of ~450 and ~1,070 base pairs. PCR products were subcloned into the pGEM-T-Easy vector (Promega) and grown on agar plates for blue/white screening. Selected white colonies were grown into LB media and plasmid DNA from each culture was subjected to variant identification by size selection using agarose gel electrophoresis. DNA sequencing was used to confirm variants and exon-exon junctions. DNA sequences were compared with published rat Ca_v3.2 cDNA sequences (NM_153814) and genomic sequences (ENSRNOT00000048392 and NC_005109).

Construction of cDNA libraries and full length splice variant screening. Full-length PCR was performed with ELONGASE Enzyme Mix using the oligonucleotides 5'-GAT AAG CTT ATG ACC GAG GGC ACG-3' and 5'-CGC TCT AGA CTA CAC AGG CTC ATC-3'. The reaction volume was 50 μL consisting of 2 μL cDNA, 2 mM magnesium, 200 μM each dNTP, 400 nM each primer and 1 unit ELONGASE Enzyme Mix. PCR was run using the following cycle: 94.5°C 45 seconds, 94.5°C 20 seconds, 55°C 25 seconds, 68°C 8 minutes, 35 cycles and a final extension of 68°C for 15 minutes. The ~7 kb PCR product was purified and subcloned into the pGEM T-Easy vector. Individual splice variants from bacterial colonies obtained from short amplicon PCR products were identified via size differentiation using agarose gel electrophoresis. Between 40 and 200 colonies were screened in each of the 11 PCR reactions. For full length screening, positive full length clones were screened using *HindIII* and *SpeI* enzymes to release the ~7 kb Ca_v3.2 fragment. The identification and confirmation of alternatively spliced variants were performed by DNA sequencing 56 atria and 50 ventricular full length cDNAs.

All DNA sequences were aligned against published mRNA and genomic sequences (Ensembl and PubMed).

Cloning of full-length Ca_v3.2 alternative splice variants. Eight full-length splice variants were subcloned for subsequent biophysical characterization in HEK cells; Ca_v3.2(-25), Ca_v3.2(+25), Ca_v3.2(8b/-25), Ca_v3.2(20a/-25), Ca_v3.2(33a/-25), Ca_v3.2(Δ214/-25), Ca_v3.2(35a/-25) and Ca_v3.2(35a/+25). From the error-free full length cDNA subcloned in pGEM T-Easy vector, all Ca_v3.2 splice variants except Ca_v3.2(8b/-25) were cloned by cutting the ~7 kb band with *HindIII* and *XbaI* restriction enzymes and moved to pCDNA3.1 zeo(+) (Invitrogen). Using Ca_v3.2(-25) as template, Ca_v3.2(8b/-25) was cloned using two-step overlapping PCR techniques. Ca_v3.2(8b) alternative splice variant is 99 amino acid deletion located in the I-II linker region within the *NheI* sites of Ca_v3.2(-25) in pCDNA3.1 zeo(+). All PCR reactions were done using Phusion Enzyme (Finnzymes, Espoo, Finland). Two overlapping PCR fragments namely *NheI*-8b1 and 8b2-*NheI*4 were generated. *NheI*-8b1 fragment was amplified with oligonucleotides RA1HLDHNhe1-5'-GGT CTA TAT AAG CAG AGC T-3' and RA1HLDH8b1-5'-CTC AGA GTC TGG TGG CCC ATG GCC TAC ATA CTT GAG GAG CTC C-3', whereas, 8b2-*NheI*4 fragment with primers RA1HLDH8b2- 5'-GGA GCT CCT CAA GTA TGT AGG CCA TGG GCC ACC AGA CTC TGA G-3' and RA1HLDHNhe4-5'-TTC AGG CTG AAC TTA CAG CC-3'. Products were then run in 0.8% agarose gel, excised and purified for subsequent annealing. The two fragments were annealed using the oligonucleotides RA1HLDHNhe1-5'-GGT CTA TAT AAG CAG AGC T-3' and RA1HLDHNhe2-5'-CGA CTC ACT ATA GGG AGA C-3' to generate the 2.5 kb fragment possessing *NheI* sites for cutting. Annealed products were gel purified and the Ca_v3.2(-25) and the purified 8b *NheI* fragment were cut with *NheI* restriction enzymes for subsequent cloning. The 8b *NheI* fragment splice variant was cloned into the *NheI* cut Ca_v3.2(-25) in pCDNA3.1 zeo(+). The DNA sequence of each clone was determined prior to patch clamp analysis.

Western blot analysis. Protein sample extraction from heart tissue was performed by grinding frozen tissue in liquid nitrogen in extraction buffer (0.1 M Tris pH 6.8, 2% SDS, 10% Glycerol, 1% BME, 1x Proteinase inhibitor cocktail [Complete-EDTA free, Roche], 0.004% Bromophenol Blue) and followed by heating to 65°C for 10 minutes and trituration through a high gauge needle. Western Blot analysis was performed as follows: proteins were separated on NuPAGE Novex 4–12% Bis-Tris Midi gells (Invitrogen), followed by wet electro-transfer (20 mmol/L Tris-base, 150 mmol/L Glycine, 20% Methanol and 0.1% SDS) onto nitrocellulose membrane (Hybond-ECL, GE Healthcare). Protein transfer was confirmed by Ponceau S staining, followed by membrane blocking with 2% skimmed milk in TBST (136 mM NaCl, 25 mM Tris-HCl (pH 7.4), 2.8 mM KCl, 0.1% Tween). Antibody incubations were performed in TBST-2% milk for 1 hour and washed three times (5 minutes each) with TBS prior to incubation with secondary HRP conjugated antibody. Final membrane washes were performed twice in TBST and once in TBS for 5 minute each. Proteins were detected using the SuperSignal West Pico Chemiluminescent kit

(Thermo Scientific) on Hyperfilm ECL (GE Healthcare). The following antibodies used: Rabbit anti-rat Ca_v3.1 (1:10,000) (C-terminal region residues 1,861–1,934 (Q54898)), rabbit anti-rat Ca_v3.2 (1:5,000) (II-III linker region residues 11,195–1,273 (Q9EQ60)), rabbit anti-rat Ca_v1.2 (1:5,000) (C-terminal region residues 1,725–11,789 (P22002)) and mouse anti-ACTB (1:10,000) (Chemicon, MAB1501).

Quantitative real-time-PCR (qRT-PCR). Two microgram (μg) of total RNA was used to synthesize cDNA using a High Capacity cDNA Reverse Transcription kit (Applied Biosystems). Real-time-PCR reactions were performed using Applied Biosystems reagents, an Applied Biosystems AB 7500 instrument and TaqMan probes generated against the respective cDNA targets. Primer mixes used for detection of specific splice variants are listed in **Supplemental Table 2**. Splice-variant specificity was confirmed using full-length cDNAs and titration curves and enabled splice-variant copy number to be calculated. A rat actin B (rActB) primer set (Applied Biosystems AB 4352340E) was run in parallel with splice-variant specific probes in all samples as a control for total cDNA input to allow comparison. The rat molecular hypertrophic markers, SIAT7(Rn01750492_m1) and Frzb(Rn01746979_m1) were obtained from Applied Biosystems. Relative amounts of different splice variants were estimated after actin B normalization. In the case of the exon ±25 splice variants, copy numbers for each variant in each sample were calculated and then compared with rActB. Target and control probe reactions were run in triplicate and averages determined.

Whole cell electrophysiology of transfected HEK cells. Human embryonic kidney cells (HEK293; Invitrogen, #11631-017) were grown in standard Dulbecco's modified Eagle's medium (DMEM) containing 10% heat inactivated fetal bovine serum, 50 units/ml penicillin and 50 μg/ml streptomycin maintained at 37°C in a humidified incubator with 95% oxygen and 5% CO₂. Ca_v3.2 alternative splice variants were transfected using standard calcium phosphate transfection method and left overnight at 37°C incubator. As a reporter for transfection, CD8 was used at a molar ratio of 3:1. Twelve to 18 hours later, media was replaced with fresh DMEM and cells were transferred to 28°C prior to whole cell patch clamp analysis.

Macroscopic currents were recorded using Axopatch 200B amplifiers (Axon Instruments, Foster City, CA) controlled and monitored with personal computers running with pClamp software version 9 (Axon Instruments). The external recording solution composed of the following (in mM) 2 CaCl₂, 1 MgCl₂, 92 CsCl, 10 glucose, 40 tetraethylammonium chloride, 10 HEPES, pH 7.4 and the internal pipette solution contained (in mM) 120 Cs-MeSO₃, 11 EGTA, 10 HEPES, 2 MgCl₂, 5 MgATP, pH 7.2. In some experiments using Ba as the charge carrier, Ca was replaced with iso-osmotic external recording solution containing barium. Patch pipettes (borosilicate glass BF150-86-10; Sutter instruments, Novato, CA) were pulled using a Sutter P-87 puller and fire polished with a Narashige (Tokyo, Japan) microforge with typical resistances of 3–6 MΩ when filled with internal solution. The bath was grounded via a 3 mol/L KCl bridge. Data were low pass filtered at 2 kHz except for measurement of tail

currents that were filtered at 5 kHz with built-in Bessel filter of the amplifier, with a sampling period of 10 kHz.

Voltage dependence of activation was studied by applying 150 msec depolarizing pulses from -90 mV to +10 mV at 5 mV increments ($V_h = -110$ mV). Current-voltage (I-V) relationships were fitted with the modified Boltzmann equation: $I_m = \{G_{max} \times (V_m - E_{rev})\} / \{1 + \exp[(V_m - V_{50act})/k_{act}]\}$, where G_{max} is the maximum slope conductance; E_{rev} is the extrapolated reversal potential; V_m is the membrane potential, V_{50act} is the half activation potential; k_{act} is the slope factor of activation which reflects the voltage sensitivity. Current values were normalized to the maximum current. Steady-state inactivation was studied by applying 5 second prepulses from -120 mV to -10 mV followed by a test pulse to -30 mV for 50 ms. The current magnitude obtained during each test pulse was normalized to the maximum current and plotted as a function of the pre-pulse potential. Steady state inactivation normalized data were fitted using Boltzmann equation $(I/I_{max} = \{1 + \exp[(V - V_{50inact})/k_{inact}]\}^{-1})$, where I_{max} is the maximum current; $V_{50inact}$ is the membrane potential at which 50% of the channel are inactivated, k_{inact} is the slope factor of inactivation. The kinetics of activation (τ_{act}) and inactivation (τ_{inact}) were analyzed by fitting current recordings obtained from the I-V protocol with a single exponential standard equation $I = Ae^{-t/\tau}$, where A is the amplitude of the current and τ is the time constant. Recovery from inactivation was determined by double pulse protocol, a prepulse to -30 mV for 400 ms was given and allowed to recover at different time intervals (interpulse interval) between 5 ms to 5 seconds before applying a test pulse to -30 mV for 50 ms ($V_h = -110$ mV). The peak current from the test pulse was plotted as ratio of maximum prepulse current versus interval between pulses. The data were fitted with a double exponential function $[I/I_{max} = A1 \cdot \exp(-t/\tau1) + A2 \cdot \exp(-t/\tau2)]$, where A1 and A2 are the amplitude for the fast and slow components of the exponential and $\tau1$ and $\tau2$ are the time constants

for the fast and slow components, respectively. Deactivation was also investigated by measuring tail currents, using -110 mV as holding potential and depolarizations to -30 mV after which the membrane was repolarized to different levels (-120 mV to -50 mV). The data was fitted with a single exponential function ($I = A \cdot \exp(-t/\tau)$), where A is the amplitude of the current and τ is the time constant. Fittings were plotted as a function of the repolarization potential. Voltage-dependent facilitation was studied by applying a 200 ms test pulse to -30 mV following a series of depolarizing prepulses from -120 to +150 mV after a time interval of 1.2 seconds. The percentage facilitation was obtained by dividing the currents obtained from prepulses to currents recorded at -120 mV. Averaged percentage facilitation was plotted as a function of prepulse depolarization. All recordings were performed at room temperature (~22–24°C).

Data analysis was performed using Clampfit software version 9.0 (Axon Instruments). All plots and statistical analysis (ANOVA) were performed using the Microcal Origin software version 7.5 (Northampton, MA).

Acknowledgements

The work was supported by operating grants from the Canadian Institutes of Health Research and Genome BC and a Canada Research Chair in Biotechnology and Genomics-Neurobiology (to Terrance P. Snutch). Laurence S. David was supported by a doctoral research award from the Heart and Stroke Foundation of Canada. We thank Dr. Edwin Moore for helpful comments and suggestions.

Note

Supplementary materials can be found at: www.landesbioscience.com/supplement/DavidCHAN4-5-Sup.pdf

References

- Black DL. Mechanisms of alternative pre-messenger RNA splicing. *Annu Rev Biochem* 2003; 72:291-336.
- Stetefeld J, Ruegg MA. Structural and functional diversity generated by alternative mRNA splicing. *Trends Biochem Sci* 2005; 30:515-21.
- Modrek B, Lee C. A genomic view of alternative splicing. *Nat Genet* 2002; 30:13-9.
- Adams PJ, Garcia E, David LS, Mulatz KJ, Spacey SD, Snutch TP. $Ca_v2.1$ P/Q-type calcium channel alternative splicing affects the functional impact of familial hemiplegic migraine mutations: implications for calcium channelopathies. *Channels (Austin)* 2009; 3:110-21.
- Chang SY, Yong TF, Yu CY, Liang MC, Pletnikova O, Troncoso J, et al. Age and gender-dependent alternative splicing of P/Q-type calcium channel EF-hand. *Neurosci* 2007; 145:1026-36.
- Diebold RJ, Koch WJ, Ellinor PT, Wang JJ, Muthuchamy M, Wiczeorek DF, Schwartz A. Mutually exclusive exon splicing of the cardiac calcium channel $\alpha1$ subunit gene generates developmentally regulated isoforms in the rat heart. *Proc Natl Acad Sci USA* 1992; 89:1497-501.
- Lopez AJ. Alternative splicing of pre-mRNA: developmental consequences and mechanisms of regulation. *Annu Rev Genet* 1998; 32:279-305.
- Kong SW, Hu YW, Ho JW, Ikeda S, Polster S, John R, et al. Heart failure-associated changes in RNA splicing of sarcomere genes. *Circ Cardiovasc Genet* 2010; 3:138-46.
- Shang LL, Pfahnl AE, Sanyal S, Jiao Z, Allen J, Banach K, et al. Human heart failure is associated with abnormal C-terminal splicing variants in the cardiac sodium channel. *Circ Res* 2007; 101:1146-54.
- Tiwari S, Zhang Y, Heller J, Abernethy DR, Soldatov NM. Atherosclerosis-related molecular alteration of the human $Ca_v1.2$ calcium channel $\alpha1C$ subunit. *Proc Natl Acad Sci USA* 2006; 103:17024-9.
- Wärnecke C, Surder D, Curth R, Fleck E, Regitz-Zagrosek V. Analysis and functional characterization of alternatively spliced angiotensin II type 1 and 2 receptor transcripts in the human heart. *J Mol Med* 1999; 77:718-27.
- Hatano S, Yamashita T, Sekiguchi A, Iwasaki Y, Nakazawa K, Sagara K, et al. Molecular and electrophysiological differences in the L-type Ca^{2+} channel of the atrium and ventricle of rat hearts. *Circ J* 2006; 70:610-4.
- Mangoni ME, Couette B, Bourinot E, Platzer J, Reimer D, Striessnig J, et al. Functional role of L-type $Ca_v1.3$ Ca^{2+} channels in cardiac pacemaker activity. *Proc Natl Acad Sci USA* 2003; 100:5543-8.
- Mangoni ME, Traboulsie A, Leoni AL, Couette B, Marger L, Le Quang K, et al. Bradycardia and slowing of the atrioventricular conduction in mice lacking $Ca_v3.1/\alpha1G$ T-type calcium channels. *Circ Res* 2006; 98:1422-30.
- Vassort G, Talavera K, Alvarez JL. Role of T-type Ca^{2+} channels in the heart. *Cell Calcium* 2006; 40:205-20.
- Mangoni ME, Nargeot J. Genesis and regulation of the heart automaticity. *Physiol Rev* 2008; 88:919-82.
- Rosati B, Dun W, Hirose M, Boyden PA, McKinnon D. Molecular basis of the T- and L-type Ca^{2+} currents in canine Purkinje fibres. *J Physiol* 2007; 579:465-71.
- Cribbs LL, Martin BL, Schroder EA, Keller BB, Delisle BP, Satin J. Identification of the t-type calcium channel ($Ca_v3.1d$) in developing mouse heart. *Circ Res* 2001; 88:403-7.
- Ferron L, Capuano V, Deroubaix E, Coulombe A, Renaud JF. Functional and molecular characterization of a T-type Ca^{2+} channel during fetal and postnatal rat heart development. *J Mol Cell Cardiol* 2002; 34:533-46.
- Niwa N, Yasui K, Ophoff T, Takemura H, Shimizu A, Horiba M, et al. $Ca_v3.2$ subunit underlies the functional T-type Ca^{2+} channel in murine hearts during the embryonic period. *Am J Physiol Heart Circ Physiol* 2004; 286:2257-63.
- Qu Y, Boujtir M. Gene expression of SERCA2a and L- and T-type Ca channels during human heart development. *Pediatr Res* 2001; 50:569-74.

22. Huang B, Qin D, Deng L, Boutjdir M, N E-S. Reexpression of T-type Ca^{2+} channel gene and current in post-infarction remodeled rat left ventricle. *Cardiovasc Res* 2000; 46:442-9.
23. Martinez ML, Heredia MP, Delgado C. Expression of T-type Ca^{2+} channels in ventricular cells from hypertrophied rat hearts. *J Mol Cell Cardiol* 1999; 31:1617-25.
24. Nuss HB, Houser SR. T-type Ca^{2+} current is expressed in hypertrophied adult feline left ventricular myocytes. *Circ Res* 1993; 73:777-82.
25. Takebayashi S, Li Y, Kaku T, Inagaki S, Hashimoto Y, Kimura K, et al. Remodeling excitation-contraction coupling of hypertrophied ventricular myocytes is dependent on T-type calcium channels expression. *Biochem Biophys Res Commun* 2006; 345:766-73.
26. Yasui K, Niwa N, Takemura H, Ophof T, Muto T, Horiba M, et al. Pathophysiological significance of T-type Ca^{2+} channels: expression of T-type Ca^{2+} channels in fetal and diseased heart. *J Pharmacol Sci* 2005; 99:205-10.
27. Chiang CS, Huang CH, Chieng H, Chang YT, Chang D, Chen JJ, et al. The $\text{Ca}_v3.2$ T-type Ca^{2+} channel is required for pressure overload-induced cardiac hypertrophy in mice. *Circ Res* 2009; 104:522-30.
28. Chemin J, Monteil A, Bourinet E, Nargeot J, Lory P. Alternatively spliced $\alpha(1G)$ ($\text{Ca}_v3.1$) intracellular loops promote specific T-type Ca^{2+} channel gating properties. *Biophys J* 2001; 80:1238-50.
29. Chemin J, Monteil A, Dubel S, Nargeot J, Lory P. The $\alpha 1I$ T-type calcium channel exhibits faster gating properties when overexpressed in neuroblastoma/glioma NG 108-15 cells. *Eur J Neurosci* 2001; 14:1678-86.
30. Emerick MC, Stein R, Kunze R, McNulty MM, Regan MR, Hanck DA, et al. Profiling the array of $\text{Ca}_v3.1$ variants from the human T-type calcium channel gene CACNA1G: alternative structures, developmental expression and biophysical variations. *Proteins* 2006; 64:320-42.
31. Jagannathan S, Punt EL, Gu Y, Arnoult C, Sakkas D, Barratt CL, et al. Identification and localization of T-type voltage-operated calcium channel subunits in human male germ cells. Expression of multiple isoforms. *J Biol Chem* 2002; 277:8449-56.
32. Mittman S, Guo J, Emerick MC, Agnew WS. Structure and alternative splicing of the gene encoding $\alpha 1I$, a human brain T calcium channel $\alpha 1$ subunit. *Neurosci Lett* 1999; 269:121-4.
33. Murbartian J, Arias JM, Lee JH, Gomora JC, Perez-Reyes E. Alternative splicing of the rat $\text{Ca}_v3.3$ T-type calcium channel gene produces variants with distinct functional properties(1). *FEBS Lett* 2002; 528:272-8.
34. Ohkubo T, Inoue Y, Kawarabayashi T, Kitamura K. Identification and electrophysiological characteristics of isoforms of T-type calcium channel $\text{Ca}_v3.2$ expressed in pregnant human uterus. *Cell Physiol Biochem* 2005; 16:245-54.
35. Zhong X, Liu JR, Kyle JW, Hanck DA, Agnew WS. A profile of alternative RNA splicing and transcript variation of CACNA1H, a human T-channel gene candidate for idiopathic generalized epilepsies. *Hum Mol Genet* 2006; 15:1497-512.
36. Powell KL, Cain SM, Ng C, Sirdesai S, David LS, Kyi M, et al. A $\text{Ca}_v3.2$ T-type calcium channel point mutation has splice-variant-specific effects on function and segregates with seizure expression in a polygenic rat model of absence epilepsy. *J Neurosci* 2009; 29:371-80.
37. Vitko I, Bidaud I, Arias JM, Mezghrani A, Lory P, Perez-Reyes E. The I-II loop controls plasma membrane expression and gating of $\text{Ca}_v3.2$ T-type Ca^{2+} channels: a paradigm for childhood absence epilepsy mutations. *J Neurosci* 2007; 27:322-30.
38. DePuy SD, Yao J, Hu C, McIntire W, Bidaud I, Lory P, et al. The molecular basis for T-type Ca^{2+} channel inhibition by G protein $\beta 2\gamma 2$ subunits. *Proc Natl Acad Sci USA* 2006; 103:14590-5.
39. Wolfe JT, Wang H, Howard J, Garrison JC, Barrett PQ. T-type calcium channel regulation by specific G-protein $\beta\gamma$ subunits. *Nature* 2003; 424:209-13.
40. Gomora JC, Murbartian J, Arias JM, Lee JH, Perez-Reyes E. Cloning and expression of the human T-type channel $\text{Ca}_v3.3$: insights into prepulse facilitation. *Biophys J* 2002; 83:229-41.
41. Klockner U, Lee JH, Cribbs LL, Daud A, Hescheler J, Pereverzev A, et al. Comparison of the Ca^{2+} currents induced by expression of three cloned $\alpha 1$ subunits, $\alpha 1G$, $\alpha 1H$ and $\alpha 1I$, of low-voltage-activated T-type Ca^{2+} channels. *Eur J Neurosci* 1999; 11:4171-8.
42. Cerutti C, Kurdi M, Bricca G, Hodroj W, Paultre C, Randon J, et al. Transcriptional alterations in the left ventricle of three hypertensive rat models. *Physiol Genomics* 2006; 27:295-308.
43. Zhao M, Chow A, Powers J, Fajardo G, Bernstein D. Microarray analysis of gene expression after transverse aortic constriction in mice. *Physiol Genomics* 2004; 19:93-105.
44. Hildebrand ME, David LS, Hamid J, Mulatz K, Garcia E, Zamponi GW, et al. Selective inhibition of $\text{Ca}_v3.3$ T-type calcium channels by $\text{G}\alpha_q/11$ -coupled muscarinic acetylcholine receptors. *J Biol Chem* 2007; 282:21043-55.
45. Arnoult C, Lemos JR, Florman HM. Voltage-dependent modulation of T-type calcium channels by protein tyrosine phosphorylation. *EMBO J* 1997; 16:1593-9.
46. Iftinca MC, Zamponi GW. Regulation of neuronal T-type calcium channels. *Trends Pharmacol Sci* 2009; 30:32-40.
47. Welsby PJ, Wang H, Wolfe JT, Colbran RJ, Johnson ML, Barrett PQ. A mechanism for the direct regulation of T-type calcium channels by Ca^{2+} /calmodulin-dependent kinase II. *J Neurosci* 2003; 23:10116-21.
48. Alvarez JL, Rubio LS, Vassort G. Facilitation of T-type calcium current in bullfrog atrial cells: voltage-dependent relief of a G protein inhibitory tone. *J Physiol* 1996; 491:321-34.
49. Ganitkevich V, Isenberg G. Stimulation-induced potentiation of T-type Ca^{2+} channel currents in myocytes from guinea-pig coronary artery. *J Physiol* 1991; 443:703-25.
50. Alvarez JL, Artiles A, Talavera K, Vassort G. Modulation of voltage-dependent facilitation of the T-type calcium current by sodium ion in isolated frog atrial cells. *Pflügers Arch* 2000; 441:39-48.
51. Adolph EF. Ontogeny of heart-rate controls in hamster, rat and guinea pig. *Am J Physiol* 1971; 220:1896-902.
52. Wahler GM, Dollinger SJ, Smith JM, Flemal KL. Time course of postnatal changes in rat heart action potential and in transient outward current is different. *Am J Physiol* 1994; 267:1157-66.
53. Wekstein DR. Heart rate of the preweanling rat and its autonomic control. *Am J Physiol* 1965; 208:1259-62.
54. Ziman AP, Gomez-Viquez NL, Bloch RJ, Lederer WJ. Excitation-contraction coupling changes during postnatal cardiac development. *J Mol Cell Cardiol* 48:379-86.
55. Leuranger V, Monteil A, Bourinet E, Dayanithi G, Nargeot J. T-type calcium currents in rat cardiomyocytes during postnatal development: contribution to hormone secretion. *Am J Physiol Heart Circ Physiol* 2000; 279:2540-8.
56. Artman M, Henry G, Coetzee WA. Cellular basis for age-related differences in cardiac excitation-contraction coupling. *Prog Pediatr Cardiol* 2000; 11:185-94.
57. Welling A, Ludwig A, Zimmer S, Klugbauer N, Flockerzi V, Hofmann F. Alternatively spliced IS6 segments of the $\alpha 1C$ gene determine the tissue-specific dihydropyridine sensitivity of cardiac and vascular smooth muscle L-type Ca^{2+} channels. *Circ Res* 1997; 81:526-32.
58. Liao P, Yong TF, Liang MC, Yue DT, Soong TW. Splicing for alternative structures of $\text{Ca}_v1.2$ Ca^{2+} channels in cardiac and smooth muscles. *Cardiovasc Res* 2005; 68:197-203.
59. Liao P, Yu D, Lu S, Tang Z, Liang MC, Zeng S, et al. Smooth muscle-selective alternatively spliced exon generates functional variation in $\text{Ca}_v1.2$ calcium channels. *J Biol Chem* 2004; 279:50329-35.
60. Tang ZZ, Hong X, Wang J, Soong TW. Signature combinatorial splicing profiles of rat cardiac- and smooth-muscle $\text{Ca}_v1.2$ channels with distinct biophysical properties. *Cell Calcium* 2007; 41:417-28.
61. Tang ZZ, Liang MC, Lu S, Yu D, Yu CY, Yue DT, et al. Transcript scanning reveals novel and extensive splice variations in human I-type voltage-gated calcium channel, $\text{Ca}_v1.2$ $\alpha 1$ subunit. *J Biol Chem* 2004; 279:44335-43.
62. Liao P, Li G, Yu de J, Yong TF, Wang JJ, Wang J, et al. Molecular alteration of $\text{Ca}_v1.2$ calcium channel in chronic myocardial infarction. *Pflügers Arch* 2009; 458:701-11.